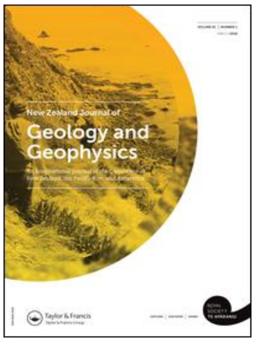

Taylor & Francis
Taylor & Francis Group

New Zealand Journal of Geology and Geophysics

ISSN: (Print) (Online) Journal homepage: https://www.tandfonline.com/loi/tnzg20

Evaluating 9 m of near-surface transpressional displacement during the M_w 7.8 2016 Kaikōura earthquake: re-excavation of a pre-earthquake paleoseismic trench, Kekerengu Fault, New Zealand

Philippa Morris, Timothy Little, Russ Van Dissen, Matthew Hill, Mark Hemphill-Haley, Jesse Kearse & Kevin Norton

NEW ZEALAND JOURNAL OF GEOLOGY AND GEOPHYSICS
https://doi.org/10.1080/00288306.2021.1954958

Taylor & Francis
Taylor & Francis Group

RESEARCH ARTICLE

Evaluating 9 m of near-surface transpressional displacement during the M_w 7.8 2016 Kaikōura earthquake: re-excavation of a pre-earthquake paleoseismic trench, Kekerengu Fault, New Zealand

Philippa Morris [a], Timothy Little[a], Russ Van Dissen[b], Matthew Hill [b], Mark Hemphill-Haley[c], Jesse Kearse[a] and Kevin Norton [a]

[a]School of Geography, Environment and Earth Sciences, Victoria University of Wellington, Wellington, New Zealand; [b]GNS Science, Lower Hutt, New Zealand; [c]Department of Geology, Humboldt State University, Arcata, CA, USA

ABSTRACT
During the Kaikōura earthquake, a paleoseismic trench was dextrally displaced ~9 m and shortened by 1.3 ± 0.4 m – the largest globally recorded displacement of a trench. Analysis showed that two processes accommodated subequal amounts of slip at the surface: (1) discrete dextral-slip on two steeply-dipping faults bounding a <3.5 m wide central deformation zone; and (2) coseismic clockwise rotation of turf rafts and pervasive sediment deformation in that zone. The second (successive) process resulted in upward (<1 m) and outward (<2 m) bulging along low-angle thrusts, creating horizontal fault-perpendicular shortening that exceeds the heave (~1.3 m). This discrepancy results from coseismic rotation of rafts, that shorten upon approaching perpendicularity with the fault – creating extra apparent shortening (in fault-orthogonal view). Comparison of pre- and post-earthquake trench logs indicates that strike-slip ruptures at the same site can be expressed differently over time; fault strands carrying major displacement in 2016 were not the locus of deformation in the previous earthquake(s), suggesting temporal unpredictability is important in defining fault zones. The last several paleoearthquakes at the trench produced cm-dm scale normal-sense dip separations across faults; however, the 2016 earthquake created compressive structures including up-bulging and low-angle reverse faulting, as well as fissuring. This contrast in deformation style likely resulted from an >8° clockwise rotation of the local slip vector in 2016 (becoming transpressive), highlighting that small changes in slip kinematics may affect rupture zone structures.

ARTICLE HISTORY
Received 9 March 2021
Accepted 5 July 2021

HANDLING EDITOR
Andy Nicol

KEYWORDS
Paleoseismology; structural geology; strike-slip faults; fault zone deformation; 2016 Kaikōura earthquake

Introduction

The M_w 7.8 Kaikōura earthquake of November 2016 in New Zealand resulted in a ~9 m dextral strike-slip displacement of a paleoseismic trench on the Kekerengu Fault that was logged and back-filled 10 months prior to the earthquake (Figures 1 and 2; Little et al. 2018). To our knowledge, this is the third time globally that a paleoseismic trench has been coseismically displaced. The first was during the Borah Peak earthquake of 1983 (Idaho, United States), when a normal fault (Lost River Fault) displaced a 7-yr old trench by 2 m (Haller et al. 2004). Parts of this trench were re-logged, and the location and style of the 1983 slip on the exposed wall was found to be similar to that which occurred during older paleoearthquakes. During the 2016 Kumamoto earthquake in Japan, two trenches were laterally displaced by ~0.5 m, but neither was re-excavated (Shirahama et al. 2016).

In this paper, we use the well-documented offset of the Kekerengu Fault paleoseismic trench (Little et al. 2018), and information logged during its re-excavation to identify and quantify the partitioning of ground deformation during a large magnitude, mostly strike-slip coseismic displacement. Both halves of the original (now displaced) trench were exhumed and re-logged, allowing pre- and post-earthquake views of identical segments of trench wall to be compared in three dimensions. Data used in this paper to infer the distribution of coseismic deformation and fault slip during the earthquake include: (1) pre-earthquake (original) trench logs and photographs (Little et al. 2018); (2) post-earthquake trench logs and photographs for the same walls as documented in the original trench; (3) pre- and post-earthquake aerial photography as well as digital surface models (DSMs) derived from those images by photogrammetry and (4) positions of selected survey marks both before and after the 2016 earthquake measured proximal to the trench site, including points along the perimeter of the original and displaced trenches. Our goal is to understand the processes by which a large predominantly strike-slip displacement was accommodated within the top few metres of sediment and soil during the 2016 earthquake.

CONTACT Philippa Morris pipala00017@gmail.com

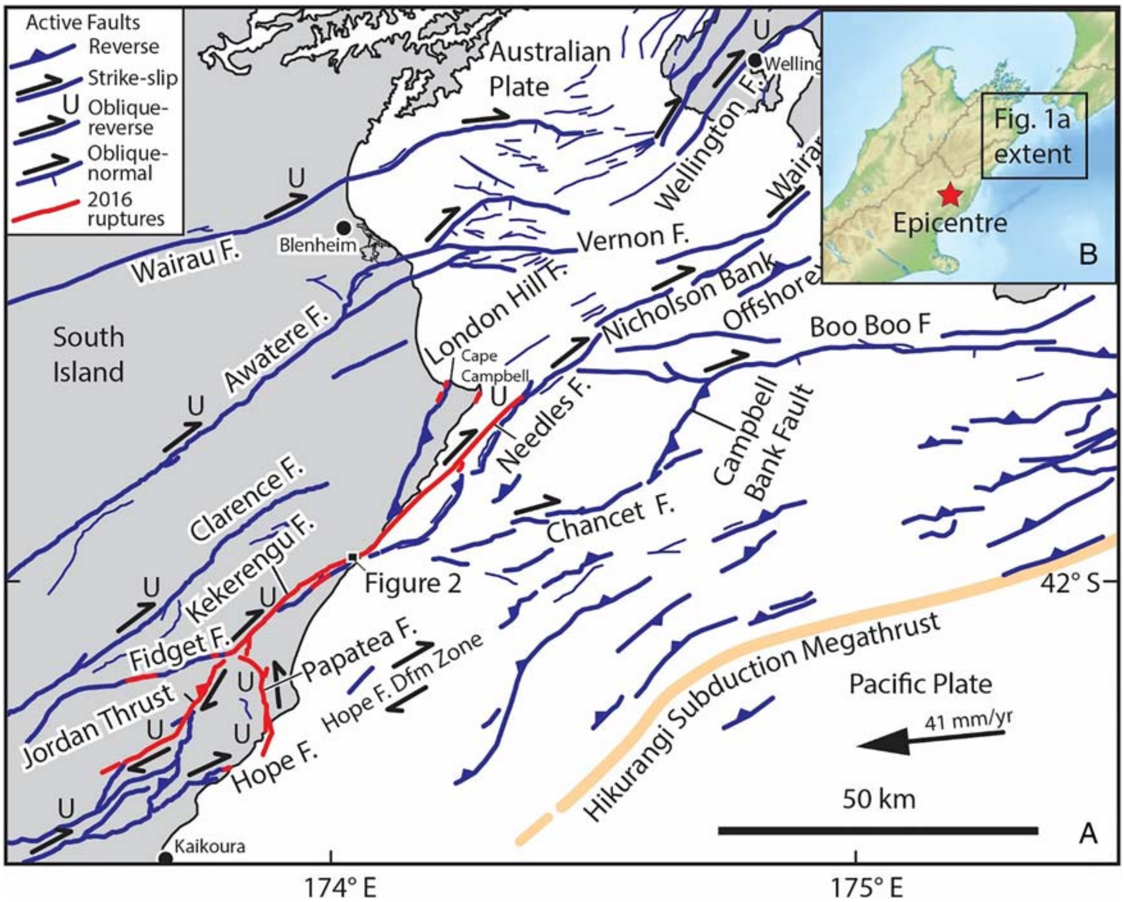

Figure 1. A, Tectonic map of the Cook Strait, between the North and South Islands of New Zealand (from Little et al. 2018). Red fault traces show the northern ruptures of the M_w 7.8 Kaikōura earthquake in 2016 (Litchfield et al. 2018). Faults that did not rupture in the 2016 earthquake are shown in blue. Location of the paleoseismic trenches from Little et al. (2018) is labelled (Figure 2); **B**, inset shows location of Figure 1a in relation to the epicentre of the M_w 7.8 Kaikōura earthquake (red star, location from Stirling et al. 2017).

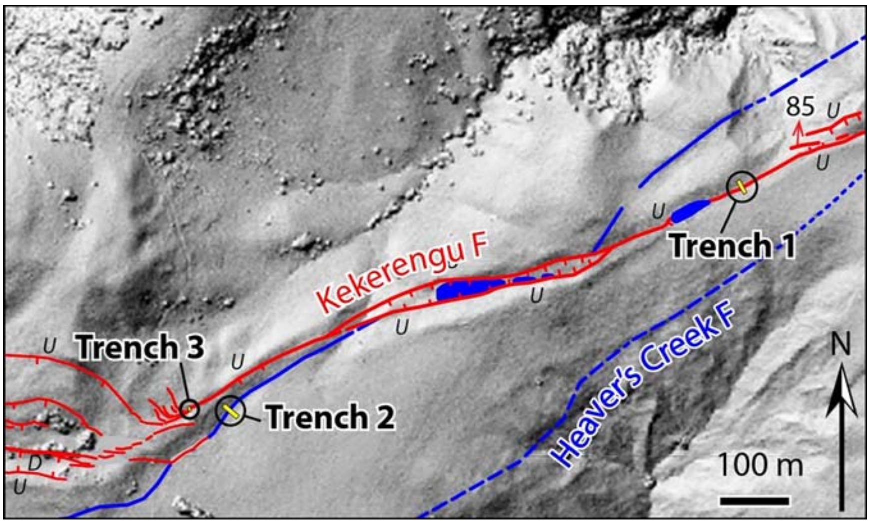

Figure 2. Map of fault traces near the three paleoseismic trenches excavated prior to the earthquake in January 2016 (adapted from Little et al. 2018). Red traces show faults that ruptured during the 2016 earthquake, while blue traces show faults that did not rupture in 2016. Blue polygons show sag ponds along the fault. See Figure 1 for location. Background is shaded DSM derived from analysis of 2014–2015 LINZ aerial imagery, gridded at 1 m (Hill and Ashraf 2017).

Background and previous work

The trench that was dextrally displaced by ~9 m by the Kekerengu Fault during the 2016 earthquake was one of three paleoseismic trenches along that fault that had been excavated by Little et al. (2018) (Figures 1 and 2). Trench 1 showed a conspicuous strike-slip

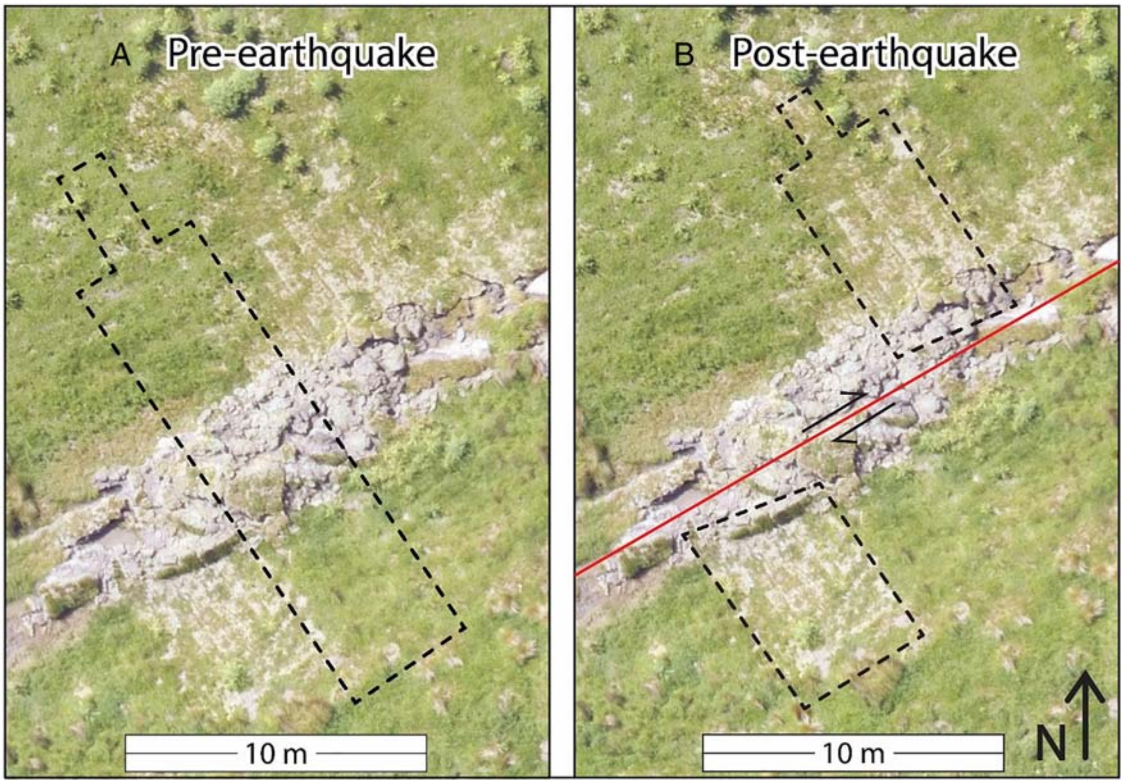

Figure 3. Map showing differential GPS-determined location of the walls of **A**, the pre-earthquake trench T1 (Figure 2) that was excavated in January 2016 (dashed black lines) and **B**, the post-earthquake locations of these margins as surveyed on 28/11/2016 by Zekkos et al. (2018) after ~9 m of dextral displacement. Simplified fault trace is shown with strike-slip arrows. Background post-earthquake (26/11/2016) orthophotograph is from Zekkos et al. (2018). Note, existing pre-earthquake aerial photography for this site is not detailed enough to show the trench site at this scale.

displacement (Figure 3). Straddling an active fault strand that did not rupture in 2016, Trench 2 was undisplaced. Trench 3, a smaller excavation, was dextrally displaced however it was effectively destroyed by dispersed ground deformation. In this paper, we will focus on the stratigraphy and coseismic deformation of Trench 1 that was uniquely preserved and is the only trench for which we can match detailed pre- and post-earthquake datasets.

Pre-earthquake trench log of T1: stratigraphy, structure and paleoearthquakes (refer to Figure 4, and Appendix A1 in Supplementary Material)

Only the southwest wall of T1 was originally logged in detail (Figure 4) prior to the earthquake in 2016, due to progressive wall-collapse soon after excavation. Near the centre of this wall, a ~2 m wide, trough-shaped fault furrow, cut by a series of steeply dipping faults (displaying components of normal displacement), marked the main fault zone of the Kekerengu Fault. The closed-drainage depression at the site of the trench had been a longstanding depocentre, accumulating organic and clay-rich sediments over several surface-rupturing paleoearthquakes at the site during the past ~1200 years (Little et al. 2018). The variably tilted and deformed limbs of this synclinal depression steepened structurally downward into older units; relationships attributed to the incremental effect of multiple paleoearthquakes, each one deepening the basin and causing renewed tilting and faulting. As observed before the 2016 earthquake, the basin had first been infilled by a layer of clayey silt (unit *uc*), and later by three peaty units (from bottom to top: units *lp*, *mp* and *up*). The fault furrow was cut by an array of at least five dextral-normal faults. Importantly, some of these faults terminated upward into the stratigraphic units: faults 3 and 4 into unit *uc*; fault 5 cut unit *lp* but not the overlying *mp* unit; and faults 1 and 2 cut the *mp* unit, but the *up* unit drapes unbroken across them (Figure 4). Wherever possible, the names of these five faults will be retained later in this paper, where the post-earthquake version of the same trench wall is described and we attempt to correlate these older structures to the post-earthquake ones. The observed dip separations of these variably and sequentially faulted units was cm-dm in magnitude, and on the basis of this incremental deformation (including the above-mentioned progressive tilting), Little et al. (2018) identified three paleoearthquakes in the pre-2016 trench walls. From oldest to youngest, these were called E3, E2 and E1. The 2016 earthquake, which took place prior to publication of that paper, was called E0.

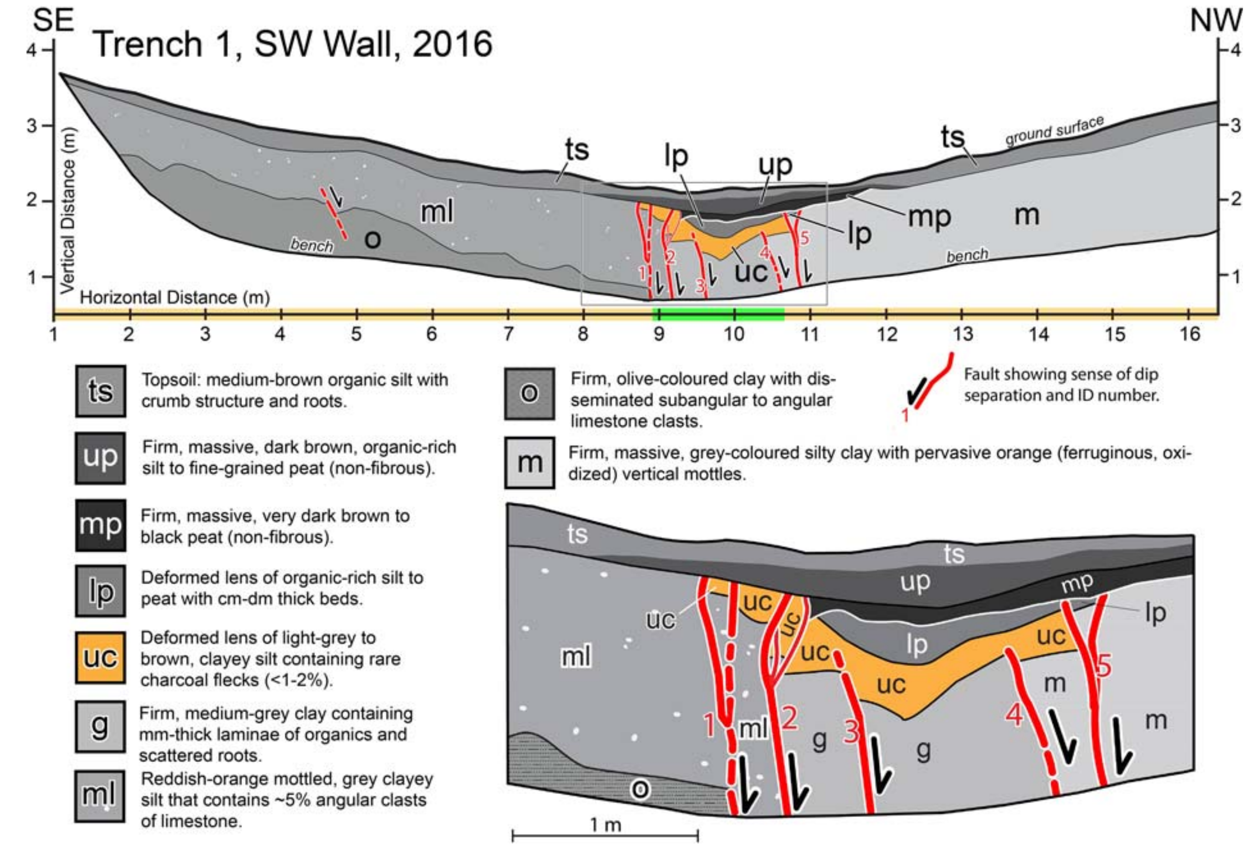

Figure 4. Pre-earthquake trench log of Trench 1 (SW wall) from Little et al. (2018), showing numbered faults (referred to in text) and mapped stratigraphic units. Only the upper ~2 m of the original trench is shown here (down to the original bench) as this is the depth to which the trench was re-excavated in 2018 as part of the present study. The northwestern end of the original trench log is excluded, because this part of the trench was little deformed in 2016, and is not discussed in the current study. Orange bars along the scale at the base of the trench identify the horizontal extent of material that was also logged in the corresponding post-earthquake trench (2018). Lime green bar underneath the central part of the log represents the central deformation zone (CDZ) of 2016, which was highly deformed during the earthquake. Inset shows an enlarged version of this CDZ (see box on the main figure) so that detailed stratigraphic and structural relationships within the central synclinal depression can be more easily identified.

Contrast in ground deformation style between the previously recognised paleoearthquakes and the 2016 earthquake

Based on the repeated axial subsidence of the synclinal depression, the normal sense of dip-separation on the logged fault strands, and the rake of slickenlines observed on some of their exhumed surfaces, the sense of fault slip during each of the paleoearthquakes E1, E2 and E3 is inferred to have been dextral-normal (i.e. transtensional). This style of long-term fault motion also accords with the tectonic geomorphology of the Kekerengu Fault on both sides of the T1 site, which consisted of (m-scale) deep fault furrows that linked together a series of elongate basins, interpreted as pull-apart basins (sag ponds). In the original trench, there was no evidence for structural up-bulging of the ground surface before, during, or after any of the recognised paleoearthquakes. By contrast, rupture during the 2016 earthquake at the same site caused widespread pressure bulging ('moletracks'), the crests of which were typically raised 0.5–1.0 m above the former ground surface (Morris 2020; Little et al. 2021). During the 2016 earthquake, the synclinal depression in T1 was completely inverted (i.e. the basin was horizontally shortened and up-bulged) to form a deeply fissured pressure bulge that reached ~1 m above the ground surface (Figures 3 and 5).

This dramatic contrast in the style of ground deformation between the 2016 earthquake and the several documented recent paleoearthquakes is enigmatic. One possible explanation is that the local slip vector azimuth was more convergent at this site in 2016 than in previous earthquakes. Another possible explanation is that the mechanical properties of the soil had changed since the last paleoearthquake (at 249–108 cal. yrs. B. P., Little et al. 2018), perhaps as a result of the introduction of exotic grasses by European pastoralists (arriving at circa 1840 A.D.). The timing of this introduction overlaps with the dated interseismic period between the last paleoearthquake (E1) and the 2016 earthquake (E0), thus supporting the second hypothesis. According to this idea, the exotic grasses may have caused the topsoil to become interwoven

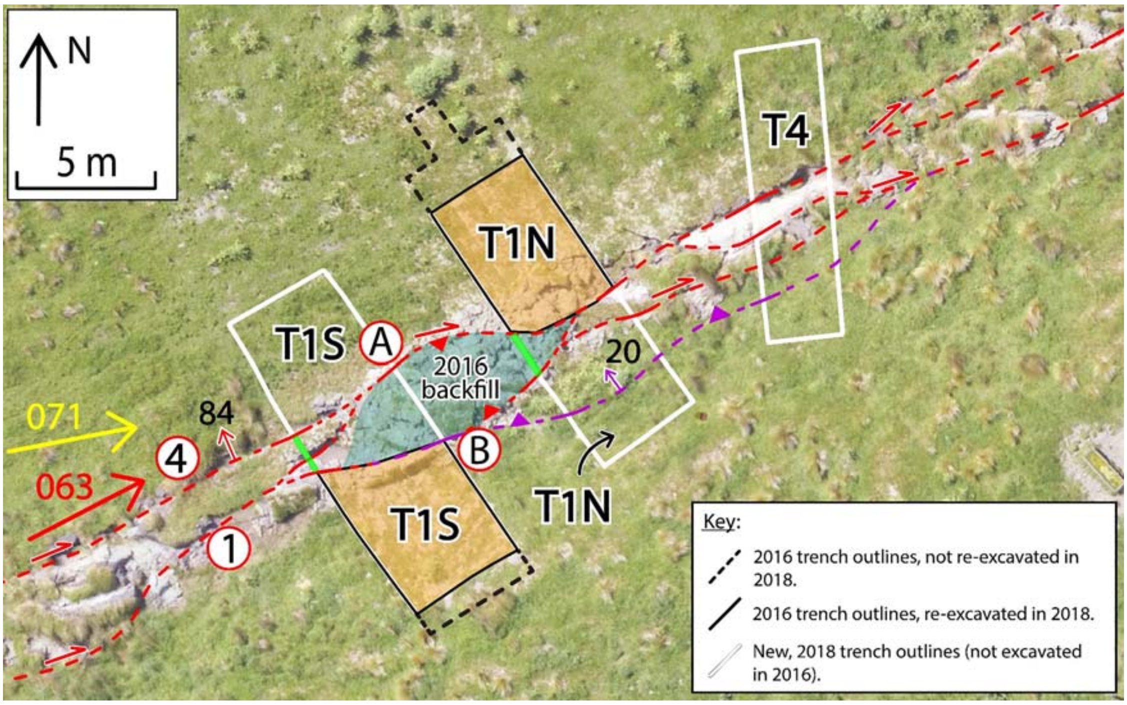

Figure 5. Post-earthquake aerial photograph of the paleoseismic trench site showing outlines of the 2018 excavations and fault traces as mapped in the post-earthquake trench logs (solid lines) and extrapolated between trenches (dashed lines). Faults coloured red accommodated primarily strike-slip motion in 2016, whereas faults coloured purple accommodated both strike-slip and reverse motion. Fault traces (red or purple) decorated by triangles indicate faults that have significant contractional heave. Arrows attached to faults denote their dip direction and dip. Numbers 1 and 4 in circles next to faults correspond to numbered faults in the trench logs of Figures 4, 7 and 9. Labels A and B adjacent to faults correlate to faults labelled in Figure 8. Black lines represent pre-earthquake trench margins (see also Figure 3), and orange shading represents the displaced halves of this original trench, labelled T1S (southern half) and T1N (northern half). White lines outline the extended dimensions of the re-excavated, post-earthquake trenches (T1N, T1S), and also the perimeter of the entirely new trench (T4). In the central part of the 2016 rupture zone, the blue shading shows the location of the earthquake-deformed and up-bulged backfill of the original T1. Arrows on the left of the map indicate (a) the mean strike of the fault zone at this locality (red arrow, 063); and (b) the azimuth of the 2016 coseismic displacement vector at this site (yellow arrow, 071). Underlying orthophotography was taken on 28/11/2016 by remotely piloted aircraft by Zekkos et al. (2018).

into a tightly bound shallow root mat, while the shallow sediment and soil may have become less granular and more clay-rich. If so, an associated increase in soil cohesion may have promoted moletrack formation in 2016. These explanations for the change in coseismic ground deformation style are discussed later on in this paper.

General approach to exhuming (and enlarging) the displaced paleoseismic trench

Re-excavation of the two displaced halves of the original trench was undertaken in February 2018 (Figure 5). This enabled us to identify the coseismically induced structural changes in its walls, by comparison of the pre- and post-earthquake trench logs and photographs. A reduced density of grass cover on the infilled ground of the original trench (artificially re-seeded following the January 2016 excavations) allowed its walls easily identified nine months after the earthquake during re-trenching. The displaced trench margin locations were confirmed by digging shallow soil pits on either side of their inferred position, and recognising the lighter colour of the backfill in comparison to the dark, undisturbed topsoil that remains outside of the trench. This allowed us to locate the original trench walls to within several cm. Finally, knowing the exact dimensions and shape of the original trench margins as surveyed by GPS during the 2016 excavation (Little et al. 2018), allowed location of segments of the post-earthquake trench perimeter that were not otherwise obvious.

The displaced halves of the T1 trench were (1) re-excavated on the north (T1N) and south (T1S) sides of the fault; and (2) lengthened along their axes into ‘new ground’ on the opposite side of the fault, to embrace the full width of the 2016 deformation zone (Figure 5). Several metres northeast along fault strike from T1N, an entirely new trench (T4, Figure 5) was also excavated at right angles to Riedel faults with the goal of better understanding the internal structure of the up-bulged moletrack. Each of these new trench margins were scraped, cleaned, gridded, photographed and logged at a scale of 1:20.

Analysis of displacement partitioning during the 2016 earthquake, through comparison of pre- and post-earthquake datasets

Revised coseismic displacement vector at the trench site

Kearse et al. (2018) estimated the coseismic slip vector near T1 by re-surveying displaced fence posts using the Real-Time Kinematic Global Positioning System (RTK GPS) technique. These markers were originally surveyed 10 months prior to the earthquake during the trenching campaign reported on in Little et al. (2018), and again shortly after the earthquake (see Appendix A2 in the Supplementary Material), where they documented 9.4 ± 0.2 m of dextral displacement. In this paper, we calculate a slip vector that is more specific to the T1 site, using: (a) the observed dextral strike-slip offset of the original trench margins as measured parallel to the 063-trending fault trace (9.0 ± 0.3 m, see Figure 6a); and (b) the fault-perpendicular horizontal convergence, or heave (1.3 ± 0.4 m), by identifying the pre- and post-earthquake position of markers on both sides of the fault, and measuring their change in position perpendicular to the fault trace (see Figure 6b, methods outlined in Appendix A2 in the Supplementary Material).

The trigonometric combination of the dextral strike-slip and heave measurements defines a horizontal displacement vector for the site that trends 071° (Figure 5). Relative to the mean fault strike of 063 at the trench site, this trend describes a moderately transpressional (convergent) displacement vector angle (α) of +8°. The measurement indicates that the trend of the slip vector in 2016 rotated clockwise by at least 8° to change from what Little et al. (2018) infer to have been a transtensional angle ($\alpha \leq 0°$) during the youngest paleoearthquake (causing E1, and basin opening and subsidence) to a transpressional one in 2016 ($\alpha = 8°$). Geomorphologically, the transition to local convergence was manifested as conspicuous up-bulging at the trench site (Figures 3 and 5).

Kearse et al. (2018) also measured 9.4 ± 0.2 m of dextral offset on a fenceline located ~20 m to the southwest of T1S, within error of our 9.0 ± 0.3 m estimate of dextral-slip as measured from offset of the trench walls. Using the fenceline, Kearse et al. (2018) showed that the coseismic dextral-slip was accommodated across a zone that was no wider than 4 m (the distance between the innermost fence posts between which the fencing wire was deformed). We note that this width is similar

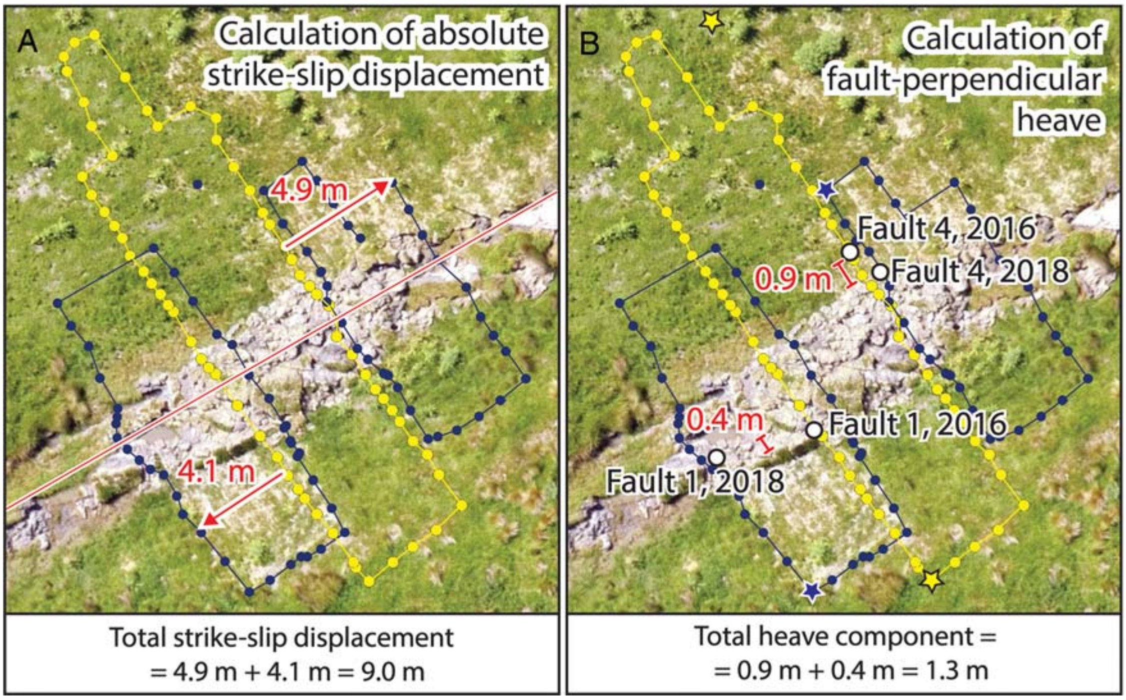

Figure 6. RTK GPS points of the pre-earthquake (yellow) and post-earthquake (dark blue) trench margins; **A**, shows the absolute dextral displacement of each of original trench halves (4.9 m for the northern half; 4.1 m for the southern one = total of 9.0 m). An average fault trace is shown in red. **B**, shows a measure of the fault-perpendicular contractional heave as summed across both sides of the fault. The total heave was calculated from the change in the pre- and post-earthquake position of re-located markers as measured perpendicular to the average fault trace. Fault 4 was the marker on the northern side of the fault; fault 1 was the marker on the southern side of the fault. Side-specific heaves (0.9 on the northern side; 0.4 on the southern = total 1.3 m) were measured as the reduction in the distance between the marker and a reference point on the outer end of that trench half. The location of the reference points are shown as stars (blue star, 2018; yellow star, 2016). The marker locations on the trench logs are shown as open circles labelled at both their 2016 and 2018 locations.

to that of the up-bulged zone at the trench site after the 2016 earthquake (Figures 3 and 5).

Post-earthquake stratigraphy and structure of the t1 trench (refer to Appendix A1 in Supplementary Material)

To further characterise the deformation components and style at the trench site resulting from 2016 rupture, it is important to identify specific structures and stratigraphic units in the 2018 trenches that were also logged prior to the 2016 earthquake. Such matched features include: (a) the five primary faults (mentioned previously, labelled numerically); and (b) the several stratigraphic units, including peat layers, infilling the synclinal depression in the centre of T1 (Figure 4). After the 2016 earthquake, these features were modified (to varying degrees) in their shape, dip, position, thickness and/or clarity of expression, resulting from coseismic deformation. It was also important to identify specific structures and stratigraphic units in the 2018 trenches, such as pre-earthquake trench back-fill, that was not present in the original T1 trench.

Trench 1S, southwest wall

Displaced westward by 4.1 ± 0.2 m from its pre-earthquake location (an absolute measure, see Figure 5), the southern part of the southwest wall of T1S (south of fault 1) is the same material as was logged in the southern part of the original trench (other than the 2016 trench spoil), shown by orange-highlighted areas in Figures 4 and 7. On the northern side of the 2016 rupture zone beyond fault 4, T1S was extended into new material that had not been logged prior to the earthquake (Figure 7). This part of the trench wall was originally located ∼9 m to the southwest of the southern part of T1S before being laterally transported into the plane of T1 during the 2016 earthquake (Figures 6 and 7). In T1S, we recognise 5 faults that we correlate to those in the original T1 (these are labelled accordingly, compare Figures 4 and 7). The faults cut the southern limb and axis of the central structural depression. Discrete slip during the earthquake was focused on faults 1 and 4. These faults bound a highly deformed, central part of the 2016 rupture zone, in which considerable distributed (macroscopically 'ductile') deformation took place, including squeezing and up-bulging of the ground. We will refer to this highly deformed zone as the central deformation zone (CDZ). It in part overlaps with the central, peat-infilled structural depression identified in the original T1. In Figure 7, this inner, strongly deformed part of the 2016 rupture zone, between faults 1 and 4, is labelled with a lime green bar along the horizontal axis.

Fault 1 is a steeply dipping structure that bounds the southeastern margin of the 2016 CDZ (Figures 5 and 7). In the pre-earthquake trench (Figure 4), this fault had two upwardly bifurcating splays, both of

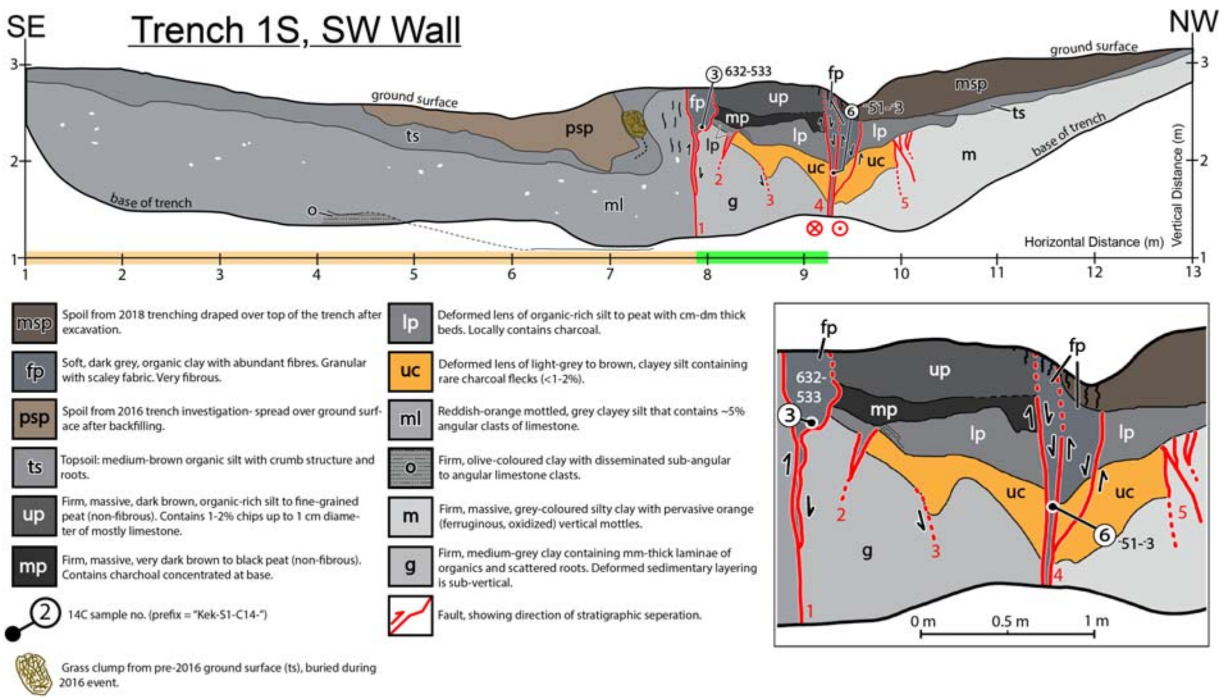

Figure 7. Post-earthquake trench log of the SW wall of Trench 1 (fragment S1, re-excavated) showing numbered faults and stratigraphic units. Faults are numbered to match their designations in the pre-earthquake trench (Figures 4 and 5). Orange bar along the scale at the base of the trench shows material that is exactly the same as that logged in the pre-earthquake (2016) trench (but contractionally deformed). Lime green bar shows the extent of the central deformation zone (CDZ), also shown enlarged in the inset. No vertical exaggeration.

which cut the *uc* unit and were overlain by an unbroken *up* unit. During the 2016 earthquake, fault 1 was reactivated as a major locus of slip, cutting upward through the previously unbroken *up* unit. Retaining its upward splaying geometry, the post-2016 version of fault 1 encloses a fault slice that appears to be a tectonic mixture of peaty units at the top of the stratigraphic sequence, including unit *lp* (the ^{14}C age of sample S1-03 is 632–533 cal. yrs. B.P – similar to previous dates for unit *lp*; see Figure 7 and Appendix A3 in the Supplementary Material). On the original trench wall between faults 1 and 2, a ∼15 cm-thick faulted slice of unit *uc* was present (Figure 4). This (probably laterally-discontinuous) slice appears to have been displaced out-of-plane during the 2016 earthquake, as it is absent in Figure 7; we infer that distributed dextral shearing adjacent to fault 1 either transported this material out-of-plane to the northeast or homogenised it beyond recognition. In addition to accommodating discrete dextral-slip at the site on fault 1 (probably 3–4 m, see below), it also accommodated considerable convergent motion during the 2016 earthquake, as indicated by the steep tilting and tight synclinal folding of the *ml* unit and its topsoil (*ts*) on its southeast side, as well as the overlying, anthropogenically introduced (in 2016) layer of pre-earthquake T1 trench spoil (unit *psp*, see Figure 7).

Sub-vertical in dip, fault 4 bounds the northwest margin of the strongly deformed part of the 2016 rupture zone at the trench site (lime green bar on Figure 7). Following the 2016 earthquake, this fault has three upwardly bifurcating splays surrounded by sheared organic rich clay (unit fp). The fault cuts through all stratigraphic units to reach the modern ground surface. Much of the material enclosed within these splays was likely derived from the 2016 topsoil (unit ts), as evidenced by the modern radiocarbon age of sample S1-06 (Figure 7 and Appendix A3 in the Supplementary Material). Interestingly, Fault 4 became a major locus of dextral-slip in 2016, even though it did not slip during the last two paleoearthquakes E1 and E2 (as evidenced by its upward termination against units *mp* and *up* in the original trench, see Figure 4).

In T1S, a >1.5 m wide zone between faults 1 and 4 (lime green bar in Figure 7) was affected by pervasive deformation during 2016. Within this zone, faults and stratigraphic units that had been identified and logged in the pre-earthquake trench were in some cases difficult to correlate to the post-earthquake trench because their geometry, dip, thickness and/or expression had changed. We attribute the changes to a mixture of strike-slip shearing and horizontal compression (and vertical up-bulging) of the deformed clay-rich materials. These deformational processes resulted in thickness changes and increased dip angles of the deformed units (Figure 7) in comparison to their pre-earthquake counterparts (Figure 4). We also infer that some material was laterally transported out-of-plane as a result of the strike-slip shearing, thus contributing to shape changes in the units. Given the >9 m of dextral-slip at the site and the lack of markers to measure strike-slip at a narrow (<1 m) spatial scale, we are unable to quantify how much the pervasive/distributed component of strike-slip contributed to this total. We infer, however that most of the contractional heave was absorbed by (1) pervasive shortening and up-bulging of material in this zone, (2) reverse slip on fault 1 with synclinal steepening of strata against its southern side and (3) analogous deformation on the opposite side of the fault (as observed in T1N, see below). For detailed descriptions of the stratigraphic changes to the CDZ, as well as the section of the trench wall to the northwest of fault 4, see Appendix A4 in the Supplementary Material.

Trench 1S, NE wall

Trench T1S (Figure 8) reoccupies the northeast wall of the southern fragment of the original trench. This wall that was not logged in 2016 prior to the earthquake because it collapsed; however, it was photographed prior to that failure (Appendix A1 in the Supplementary Material). After the 2016 earthquake, the material exposed in this trench wall is dominated by an up-bulged mass of clay-rich material (unit *tbf*). Unit *tbf* is an anthropogenic deposit consisting of chaotically mixed chunks of the T1 trench material that had been used to backfill T1 prior to the 2016 earthquake. The post-2016, deformed version of that backfill is bounded by two steep, upwardly convex faults (faults A and B on Figures 5 and 8). The distance between these two faults is <1 m at 2.5 m depth in the trench, but ∼5 m at the ground surface – a mushroom-like geometry that suggests horizontal 'squeezing' of the backfill at depth, compensated by vertical uplift and outward expansion of the material near the surface. The strongly deformed, central part of the fault zone is laterally continuous with the CDZ described on the southwest wall of the same trench fragment (Figure 7).

Fault A bounds the northwest margin of the backfill (unit *tbf*) and upwardly bifurcates into two strands midway up the trench wall. Fault A intersects along-strike with fault 4 to the southwest (see Figure 5), and together they are inferred to accommodate considerable (perhaps almost half) of the total dextral strike-slip at the trench site. In addition, fault A uplifts the backfill along its highly convex-up upper splay, emplacing its mass over the *lp* and *mp* units to the northwest. A second, more steeply dipping and structurally lower splay of fault A emplaces a slice of unit *lp* (in its hanging wall) over units *lp* and *mp*. This splay crosscuts the higher and more shallowly dipping splay in an apparently out-of-sequence manner. All of these faults formed during the 2016 earthquake.

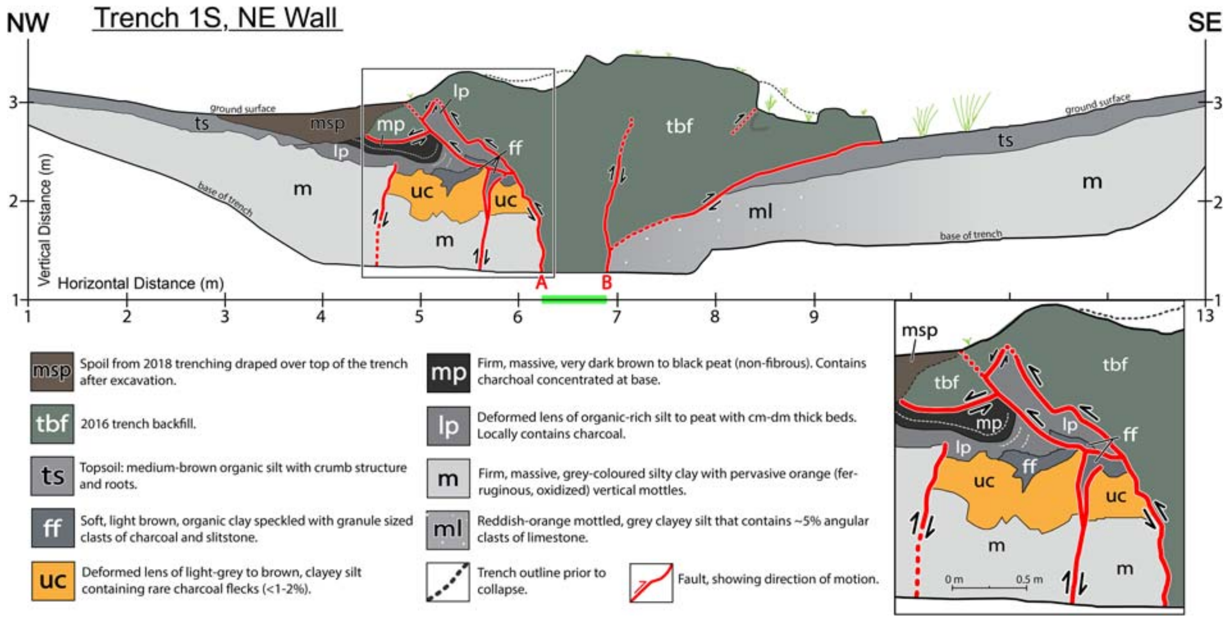

Figure 8. Post-earthquake trench log of the NE wall of Trench S1. Faults bounding the CDZ (extent shown by lime green bar) are labelled A and B (see Figure 5). Inset shows enlarged version of the displaced, original stratigraphic sequence, just to the NW of the CDZ. No vertical exaggeration.

The stratigraphy to the northwest of fault A includes peaty units of the synclinal basin that were logged in the pre-earthquake trench (Figure 4). In addition, a previously unrecognised stratigraphic unit (unit ff, organic clay) was logged on the post-earthquake trench wall, inserted between units *uc* and *lp*. We infer that during the 2016 earthquake, this lens (not present or exposed in the original trench) was transported by several metres of dextral strike-slip on fault A to occupy the plane of the post-2016 trench wall.

Near the ground surface, fault B is a low-angle (~20° dipping) fault that is inferred to have accommodated both strike-slip and convergent motion. Opposite in vergence to fault A, fault B emplaced the backfill up and over the 2016 topsoil (unit ts) to the southeast. Fault B bifurcates upward into a second, subvertical splay cutting at least part way upward though the centre of the backfill mass.

Faults A and B accommodated most of the strike-slip displacement on this trench wall, and given their proximity to T1S, we assume that they are the same structures as faults 1 and 4 in T1S and T1N.

Trench 1N, southwest wall (refer to Figure 9)

Displaced eastward (in an 'absolute' sense) by 4.9 ± 0.2 m from its pre-earthquake location (Figure 6a), the northern part of Trench 1N (Figure 9) is materially coincident with the logged northern part of the original T1 (highlighted orange in Figures 4 and 9), where it embraces part of the northern limb of the synclinal depression. Southeast of fault 4, all the material exposed on this wall was juxtaposed into the plane of the trench wall during the 2016 earthquake as a result of dextral strike-slip. This laterally introduced material does not correspond to any of the material logged in T1 before the earthquake (Figure 4).

In T1N, fault 1 at the base of the trench comprises two steep, subparallel strands that bound a slice of organic-rich sediment (units bsc, bp and usc) at a depth of ~1 m below the post-earthquake ground surface. The northern of these two steep strands bifurcates upward into two gently dipping splays: a southern, structurally lower strand (fault 1A) that shallows abruptly, displacing units *ts* (topsoil) and *ml* up and over the 2016 topsoil; and a northern, structurally higher strand (fault 1B) emplacing units *o* and *ml* over themselves in an apparent thrust repetition. Between these two fault strands is an anticlinal wedge of material capped by an overturned limb of the pre-earthquake topsoil (unit ts). While the shallow part of fault 1A accommodates a large contractional shortening (~2 m, Figure 9), we interpret fault 1 (as a whole) to have slipped with dominantly dextral motion, similar to our interpretation of that fault elsewhere (e.g. Figure 7).

Fault 4 on this trench wall is a continuation of the steeply dipping fault logged and mapped elsewhere on the northern side of the CDZ before and after the 2016 earthquake (e.g. Figures 4, 5 and 7). After the 2016 earthquake, fault 4 on this trench wall bifurcates upward into several strands that cut upward all the way to the modern ground surface, including the pre-2016 trench spoil (Figures 5 and 9). A conspicuous, downward tapering, <1 m-wide wedge of dark-coloured pre-2016 backfill (unit tbf) is enclosed between these fault strands. This fault-bounded wedge of backfill is located ~5 m northeast along

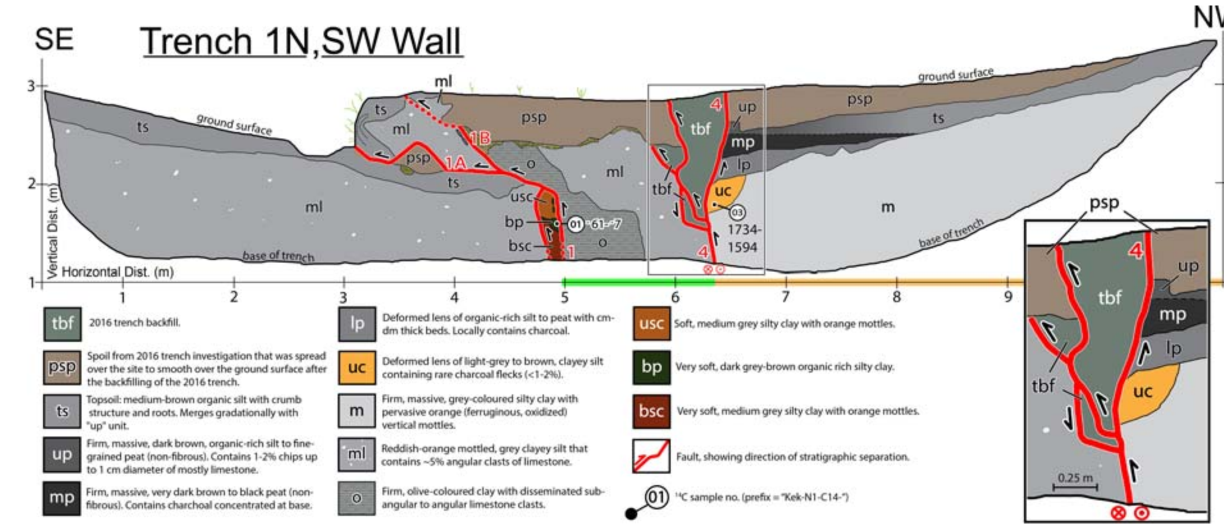

Figure 9. Post-earthquake trench log of the SW wall of Trench N1, showing numbered faults (1 and 4, correlated to the pre-earthquake trench, See Figures 4 and 5). Orange bar along the scale at the base of the trench shows material the same as that logged in the pre-earthquake (2016) trench. Lime green bar shows the extent of the CDZ. The ^{14}C age range of Sample 01 is quoted in cal. B.P. at 95% confidence (negative age is given as the sample is younger than 1950 AD). For more information on this ^{14}C sample, see Appendix A3 in the Supplementary Material. Inset shows the enlarged version of the northeastern tail end of the trench backfill from the pre-earthquake excavation (unit *tbf*), displaced into plane from the SW. Green pods sketched underneath the unit *psp* represent grass clumps from the pre-earthquake trench excavation. No vertical exaggeration.

strike from the largest accumulation of this pre-2016 material, which occurs centrally between the displaced trench halves (Figures 5 and 8). We infer it to be the eastern 'feather edge' of the deformed mass of backfill; in essence, a thin, sigmoidal tail that was sheared out laterally from the originally rectangular (in 3D, prismatic) body in the pre-earthquake trench fill.

Structural interpretation of 2016 coseismic deformation in the rupture zone of the Kekerengu Fault at the trench site

To better understand coseismic deformation in this rupture zone at the 1–10 m scale, we employed 2D area balancing in the fault-perpendicular plane, and evaluated coseismic vertical motions near the trench site through differencing of pre- and post-earthquake digital surface models (DSMs). We also palinspastically reconstructed the trench walls to an intermediate state to illustrate some of the deformationally induced changes to the stratigraphy that we discussed above (refer to Appendix A5 in the Supplementary Material for these reconstructions).

Area balancing

At the trench site, contractional heave (transverse component of the total horizontal fault displacement) was 1.3 ± 0.4 m based on our measurement of the reduction in the length of the trench during the 2016 earthquake. In seeming conflict with this value, the apparent magnitude of fault-perpendicular shortening (e.g. reverse heave on faults A and B of Figure 8) in the trench logs, particularly on the northeast wall of T1S, is much greater than this. To evaluate if the shortening and up-bulging of the ground in fault-transverse cross-section view can be explained as a simple and expectable consequence of the known contractional heave in that plane, we undertook 2-D area balancing of the backfill material – the original prismatic shape and volume of which is known (Figure 10). For a simple case of area being conserved in this plane, the horizontal shortening (heave in m), original depth extent of the 'squeezed' backfill (in m), and the predicted final excess area of the deformational bulge derived from that material (A_{exp}, as measured above the trace of the pre-earthquake ground surface, in m^2) are related in a simple way (see Figure 11a for explanation and governing equation). If area was not conserved (i.e. if new material was introduced into the reference plane as a result of out-of-plane motion), then the observed excess area (A_{exm}) will differ from the predicted value (Figure 11c). Note that a lack of area balancing does not imply (or require) an overall change in volume of the deformed material in the zone, only a redistribution of material into (or out of) the chosen reference plane.

After the earthquake, the final width (W_f) of the deformed backfill on this plane was 0.66 ± 0.1 m (Figure 10). The measured contractional heave (ΔS) at the trench site was 1.3 ± 0.4 m. The calculated original width of the backfill (W_0) in this plane of view is the sum of these:

$$\begin{aligned} W_0 &= W_f + \Delta S = 0.66\,\text{m} \ + 1.30\,\text{m} \\ &= 1.96 \pm 0.4\,\text{m} \end{aligned} \quad (1)$$

In this reference plane, the original depth of the trench (and therefore its backfill, Figure 4) was 2.0 ± 0.05 m

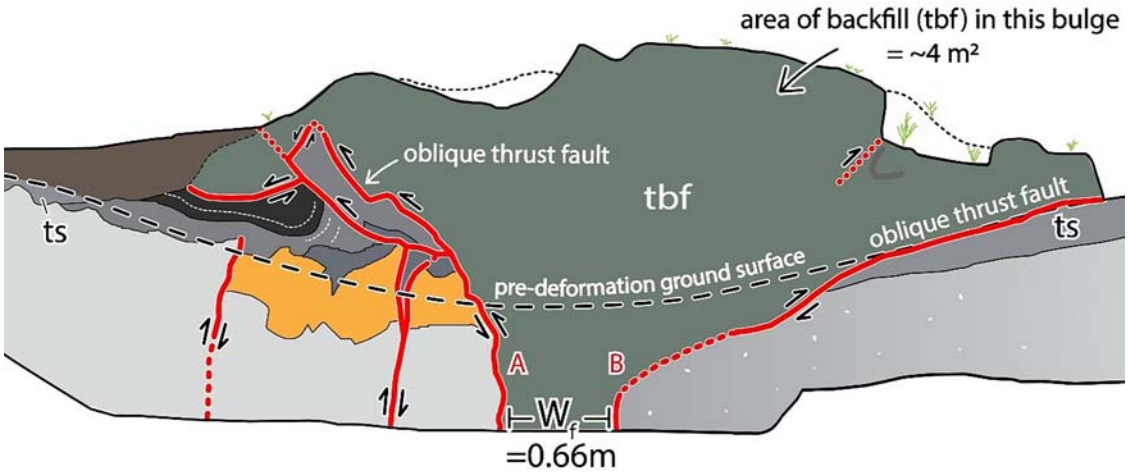

Figure 10. Enlarged version of the trench backfill (unit *tbf*) in the CDZ, as observed on the NE wall of T1S (from Figure 8). This cross-section of the coseismically deformed backfill of T1 was used to determine if area was conserved in this plane during the earthquake. Faults A and B on either side of the strongly deformed, internally sheared mass of backfill material are low-angle contractional faults (probable oblique-slip thrusts). Near the base of the trench, the deformed final width of the backfill is labelled W_f. An inferred pre-deformational ground surface is extrapolated across the trench wall along the upper contact of the topsoil where it was not bulged upward during the 2016 earthquake. The deformational excess area of the backfill lying above this pre-deformational level is ~4 m^2.

($d = 2$ m, Figure 11b). Note that while the depth at the centre of the trench extended to 4 m (Little et al. 2018), that section was very narrow (~1.5 m wide), and the chosen plane of reference was located nearer the edge of the trench, above the ~2 m deep bench. This means the basal contact for the backfill in this plane (and hence the appropriate depth for this area balancing exercise) is ~2 m. Using this depth, the original area of backfill (A_0) in the reference plane is calculated to be:

$$A_0 = W_0 \times d = 1.96\text{m} \ \times 2.0\text{m} = 3.92\text{m}^2 \pm 0.8\text{m}^2 \quad (2)$$

To predict the excess area (A_{exp}) for a case of deformational area conservation in the reference plane (Figure 11c), one multiplies the known amount of contractional heave (ΔS) by the depth of the backfill (d):

$$A_{exp} = \Delta S \times d = 1.30\text{m} \ \times 2.0\text{m} = 2.6 \pm 0.8\text{m}^2 \quad (3)$$

Based on the logged topographic profile on the NE wall of T1S (Figure 8), the actual deformational excess area of the backfill (A_{exm}) in this plane is ~4 ± 0.2 m^2 (this is the measured area of the bulge above the pre-deformational ground surface, with error calculated based on the uncertainty in our physical measurements). For $A_{exm} > A_{exp}$ requires either: (a) that our assumed depth of the backfill (d) and/or heave (ΔS) as used in the calculation were too small; or (b) that additional backfill material (area) was introduced into the plane of view during the earthquake as a result of out-of-plane motion. Such a deformational redistribution of material would be most plausibly attributed to either distributed dextral shearing and/or to clockwise vertical-axis rotation of relatively coherent, detached rafts or blocks, as documented by Morris (2020) and Little et al. (2021). It is unlikely that the parameters in scenario (a) are the reason that $A_{exm} > A_{exp}$; the depth of the backfill (d) in the original trench (T1) along the line of section is known to within ± 5 cm, and the heave (ΔS) has a measured uncertainty of ± 0.4 m, which was carried through in our calculation of the area discrepancy ($A_{exm} - A_{exp} = 1.4 \pm 0.4$ m^2), so these potential errors cannot be the chief explanation.

We conclude from this analysis that the most plausible explanation for the considerable area of the deformational bulge (Figure 10) is that material derived from out of plane has been introduced laterally into the plane of analysis by clockwise vertical-axis rotation of 'turf rafts' – a process that has been well documented for the Kekerengu Fault during the 2016 earthquake (Little et al. 2021). At the trench site, there is evidence for this in the form of elongate, fault-bounded rafts of clay and soil that appear to have rotated at least ~11° clockwise relative to the initial strike of the Riedel faults bounding them – an inception angle that is preserved in adjacent, little-deformed regions of the rupture zone (see Figure 12).

Topographic differencing

Area balancing techniques consider 2D deformational changes in a specific (in the above case, fault-perpendicular) plane of view. To better understand the coseismic deformational changes in 3D, we compare DSMs derived from processing of aerial imagery taken before the 2016 earthquake (Hill and Ashraf 2017), to those taken immediately after the earthquake by remotely piloted aerial systems (RPAS; commonly

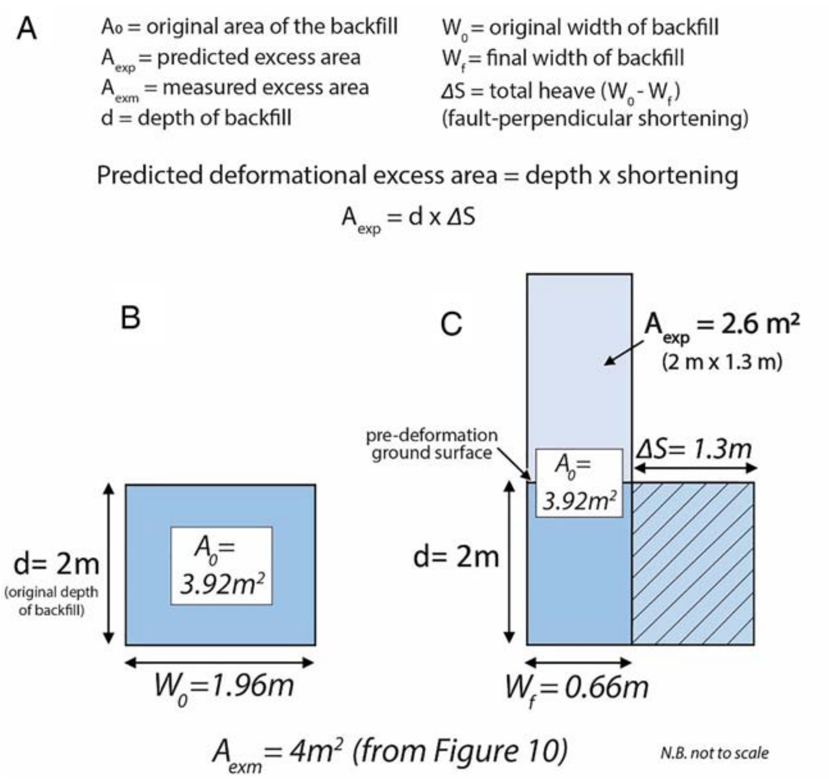

Figure 11. Diagram showing a schematic fault-perpendicular cross-sectional view of a deformational bulge, annotated with numbers relevant to Figure 10. Part **A**, shows the definitions of terms used in area balancing, and the governing equation for calculation of expected deformational excess area (A_{exp}); **B**, depicts the original area of the backfill in Figure 10 ($A_0 = 3.92$ m^2) as calculated from the known original depth of the backfill (pre-earthquake trench, $d = 2$ m) and the estimated original width of the backfill (W_0) in the plane of the cross section ($W_0 = W_f + \Delta S = 1.96$ m); **C**, shows the predicted final excess area of the backfill (A_{exp}) above a pre-deformation ground surface (labelled), after 1.3 m of shortening (assuming that the total area of 3.92 m^2 is conserved). This predicted value of excess area ($A_{exp} = 2.6$ m^2) is much smaller than the measured value ($A_{exm} = 4$ m^2, from Figure 10), by a factor of almost 50%.

known as drones), and analysed using structure-from-motion software (Zekkos et al. 2018). Differences in elevation between the two DSMs can potentially provide information about the distribution of coseismic uplift and subsidence of the ground surface in plan view. In addition, it can allow calculation of an 'excess volume' of up-bulged material in the main rupture zone relative to the pre-earthquake landscape surface. As already stated, the contractional heave (ΔS) at the site is known (1.3 ± 0.4 m). If the volume of the deformed ground materials in the rupture zone was approximately conserved during the earthquake (i.e. no significant porosity changes took place), then the accumulated 'excess volume' (V_{ex}) measured by differencing these DSMs is predicted to be:

$$V_{ex} = d \times L \times \Delta S \tag{4}$$

where L is the analysed fault strike length, ΔS is the heave, and d is the mean depth of detachment of the up-bulged material in the ~4 m-wide rupture zone (note: we do not consider farther afield vertical changes in the landscape).

The DSMs used for topographic differencing of the trench site (see Figure 13) were clipped to just the area around the paleoseismic trench. Horizontal and vertical spatial differences between the DSMs due to image georeferencing rather than earthquake-related displacement were removed. This was done by aligning artefacts such as fence posts and water troughs in the southern fault block that are in both the pre- and post-earthquake DSMs. After this alignment, the elevations of each grid cell for each surface model were sampled at a grid spacing of 20 cm (a value chosen to accommodate the differences in resolution between the two DSMs, see Figure 13) and exported as a raster image. Once loaded into Arc Map GIS, the two DSMs were differenced to produce a grid that shows the change in elevation as a result of the earthquake. Because the Kekerengu Fault slipped dextrally by ~9 m at the site, this comparison produced elevation change anomalies that were purely related to lateral motion of the topography (see Figure 13e). For example, where a ridge or hill was laterally displaced into a region where they did not formerly exist, the grid cells record a positive change in elevation, while also leaving corresponding depressions, or negative elevation changes, at their original locations.

Our most successful approach to correcting for the known ~9 m of known lateral displacement (fewest

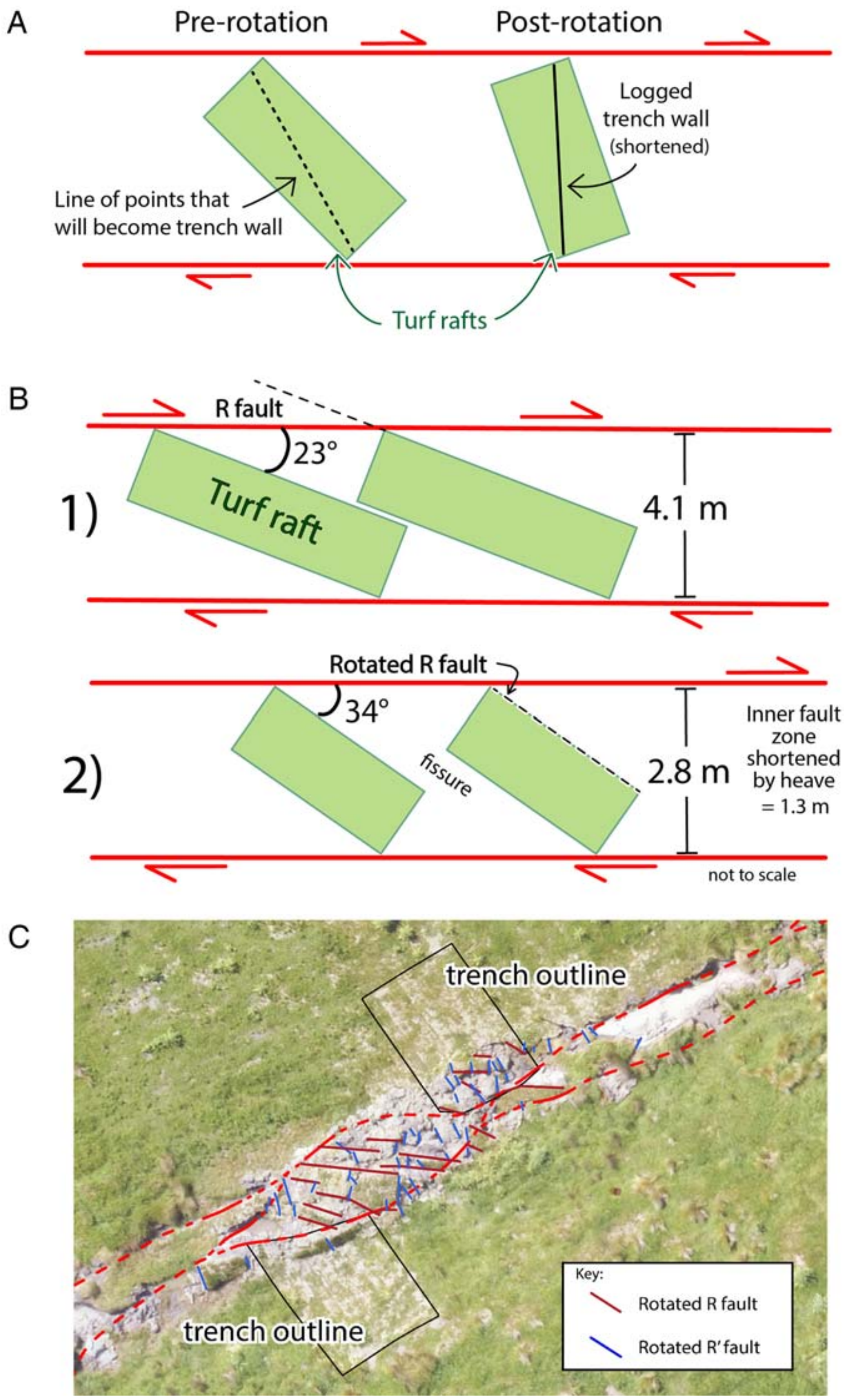

Figure 12. A, Cartoon of 'turf raft' rotation model illustrating why a line of points that ends up being rotated into the plane of the trench (perpendicular to the fault) during the earthquake is likely to be shortened – even where the overall motion has been pure strike-slip with no heave. Note that this situation predicts that extra material (area) will be introduced into the plane of the trench wall; **B**, Cartoon showing (top panel) mean pre-earthquake strike of Riedel faults and turf rafts based on observed angles in little-deformed ground to the NE of the trench site (from Morris 2020), and original width (W_0) of the up-bulged, high-strain part of the rupture zone; and (bottom panel), the corresponding final strike angle and zone width (W_f); **C**, Orthophotograph of the displaced trench site (same image as in Figure 5) showing rotated Riedel faults and turf rafts as mapped in its up-bulged rupture zone.

anomalies and artefacts, refer to Appendix A6 in the Supplementary Material for the earlier methods and their development) involved back-slipping the northern fault and the central rupture zone fault blocks in the post-earthquake DSM separately relative to the southern fault block (labelled 'Z' in Figure 14i), in an area directly surrounding the trench site. The northern block (labelled 'X') was restored by 4.5 m of westward motion on fault 4, and the central block ('Y') was restored by 4.5 m of westward motion on fault 1. This reconstruction reflects the reality that the 9 m of dextral-slip was not accommodated on a single, discrete fault, but by a combination of distributed deformation in block Y and discrete slip on the

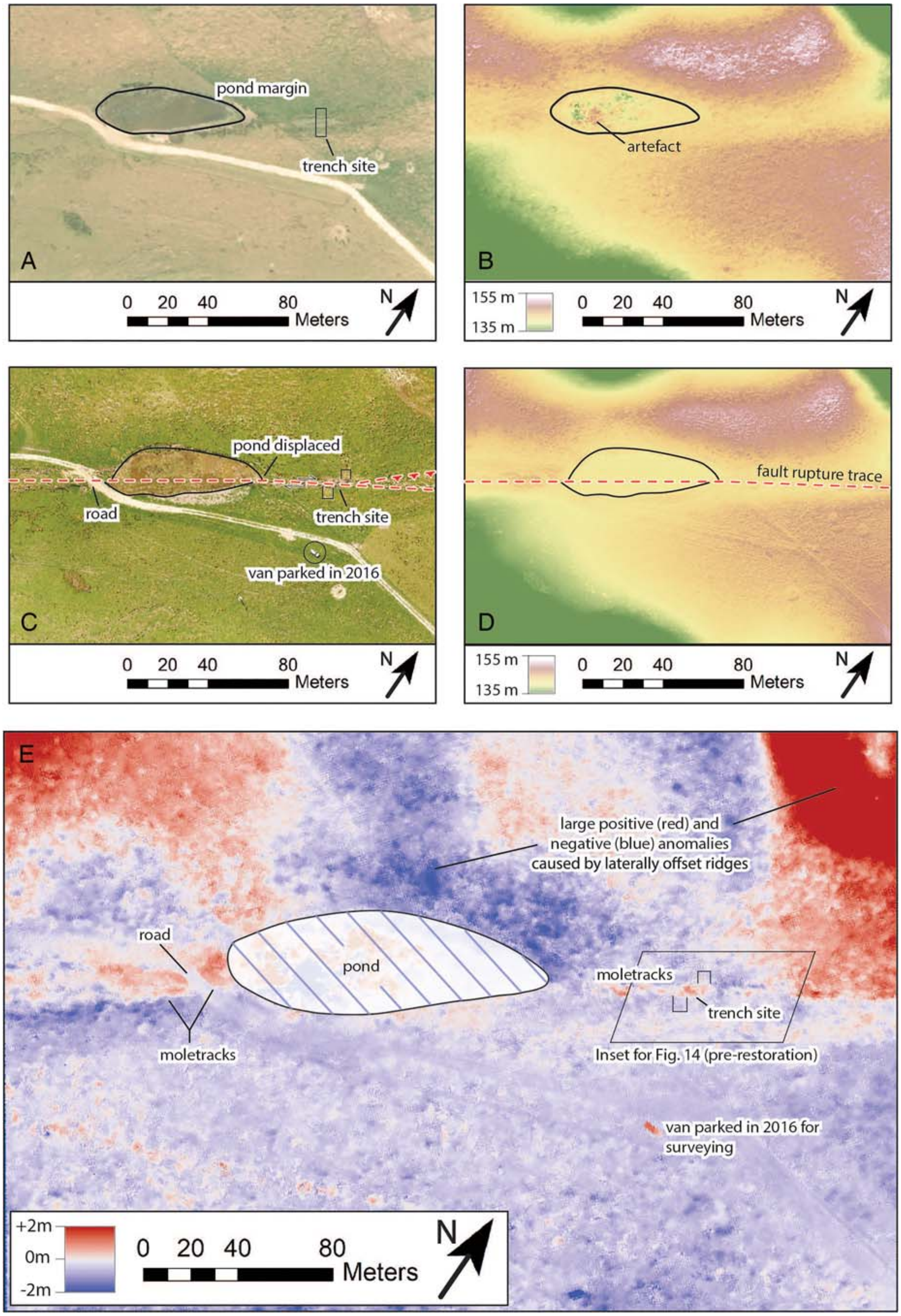

Figure 13. Orthophotographs and digital surface models (DSMs) derived from photogrammetric analysis of pre- and post-earthquake aerial imagery near the trench site were used to estimate elevation changes in the landscape. **A**, Pre-earthquake orthophotograph (2015 aerial survey, sourced from LINZ); **B**, corresponding DSM (shaded by elevation) with a grid spacing of 30 cm from Hill and Ashraf (2017); **C**, post-earthquake orthophotograph from RPAS survey (Zekkos et al. 2018) showing the main 2016 fault rupture trace and selected displaced features, including a road, pond and trench margins; **D**, corresponding DSM (shaded by elevation), with a grid spacing of 2 cm. Pre- and post- earthquake DSMs (B and D) were aligned and clipped using Cloud Compare (v2.10.2), a 3D viewing software, and then exported into ArcMap GIS where they were differenced to produce **E**, result of surface difference analaysis between the pre- and post-earthquake DSMs (range: −2 m to +2 m). Water surfaces commonly cause elevation artefacts in the photogrammetry process, and so are masked out for clarity here and not used in the analysis.

margins of that block. We also assume that the discrete slip was evenly distributed between the two faults, 1 and 4 – an inference that is consistent with the similar magnitude of 'absolute motion' experienced by the two blocks (Figure 6). When this back-shifted DSM is differenced with the pre-earthquake 2015 DSM, the restored location of the strongly up-bulged trench backfill (area of uplifted ground, shaded red, Figure 14ii) coincides with its visual location on the orthophotograph of the trench site (Figure 5). Errors in this method are derived from our uncertainty in the precise dextral-slip magnitude used in the restoration (±0.3 m), our assumption of rigid fault blocks, and the mismatch in grid sizes (resolution) between the 2015 and 2016 DSMs.

To calculate a spatially integrated value for deformational excess volume caused by mounding (and fissuring) in the rupture zone, the difference in heights from the two DSMs (which were between −2 and 2 m) were extracted in GIS and imported into a spreadsheet, using an area about ± 40 m (along-strike) from the restored trench fragments, and ± 10 m from the ends of the trenches, perpendicular to fault strike (Figure 14ii). These heights were then multiplied by the cell area in the DSM (both set at 0.2 m) to get the volume of change for each individual grid cell. The sum of these grid cell volumes was slightly negative (−341 m^3, for all ∼44,000 grid cells) at −7.8 mm^3. This net change is small given the large area for which the analysis was undertaken, indicating that to first order, the volume of ground uplifted into the bulges is balanced by the volume that subsided into fissures and other depressions during the earthquake at this location.

A negative mean change in elevation might be expected for a site that had experienced an extensional (negative) heave (ΔS); however, the trench site is known to have experienced a local contractional (positive) heave of 1.3 ± 0.4 m during the earthquake, and thus we might expect it to have generated a positive deformational excess volume (V_{ex} in Equation (4)). For an average detachment depth of 0.7 ± 0.6 m (Morris 2020), for example, and this fault length of ∼75 m, we would predict V_{ex} to be ∼70 m^3. While we cannot assign a formal uncertainty to our V_{ex} measurements, the potential errors in the calculation are large. These relate to the oversimplification in the restoration of the post-earthquake DSM, which assumes purely rigid behaviour, and the difference in cell size between the 2015 and 2016 DSMs (10 s of cm scale difference). Of the cells in the up-bulged region immediately near the trench site that showed a positive change in elevation in this differencing method (red in Figure 14ii), the average change was +9 cm^3. So, it is perhaps not surprising that an expected mean positive value for $\mathbf{V_{ex}}$ is masked amongst the larger uncertainties. The main point is that the spatially averaged uplift of the ground near the rupture was small.

While overall the mean change in elevation was negligible, by comparing the elevation changes on the northwest side of the fault to the southeast side (using the back-slipped version of the DSM shown in Figure 13), we can establish that the northwest side of the fault went up by <0.2 m compared to the southeast side.

Discussion

How and where ∼9 m of dextral slip was accommodated at the paleoseismic trench site

Through analysis of the coseismic changes between the pre- and post-earthquake data in both 2D and 3D, we have gained insight into deformational processes leading to an accumulation of 9.0 ± 0.3 m of dextral displacement and 1.3 m of contractional heave at a single well-constrained site. In the top few metres, a fraction of dextral motion was accommodated by distributed deformation of the strongly deformed, clay-rich materials within a 1.5–3.5 m-wide CDZ with the rest accommodated by discrete strike-slip on its bounding faults. Because of the absence of smaller scale linear markers, we cannot deconstruct exactly how the 9 m of strike-slip was partitioned at the metre scale between the several deformational processes in the rupture zone. Evidence for distributed shearing in the CDZ includes sheared organic-rich material in it, and stratigraphic omissions and insertions on the post-earthquake trench wall indicative of out-of-plane motion within this zone during the earthquake (i.e. tectonic juxtaposition of two spatially separated sequences). In addition to distributed shearing in the CDZ, another important contributor to distributed slip in that highly strained zone involved clockwise vertical-axis rotation of elongate turf rafts bounded by synthetic Riedel faults (Figure 12) – a mechanism documented and analysed by Little et al. (2021).

We interpret that the majority of the dextral motion at the trench site was accommodated by discrete slip on the two major ground rupturing faults on either side of the CDZ (faults 1 and 4), a conclusion that is consistent with the sharp truncation of the trench fragments against them in plan view (Figure 5), and with the apparently robust two-fault DSM reconstruction (Figure 14). In 2016, these two faults were reactivated from pre-existing (buried) faults, while other nearby faults were not reactivated. Little et al. (2021) argue that most of the Riedel faulting and their subsequent rotational deformation took place during early stages of the earthquake, accommodating 30%–50% of the dextral-slip. This near-surface rotational process was followed later in the earthquake by slip on the major ground-rupturing fault strands to accommodate the balance of the slip at ground level.

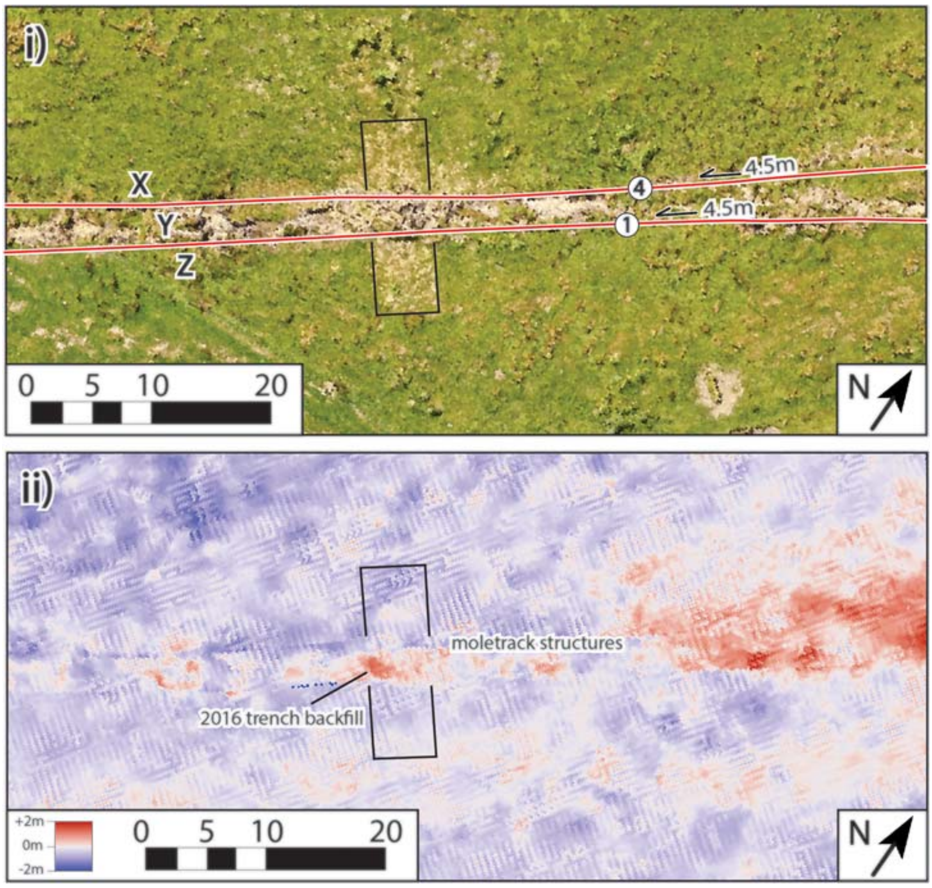

Figure 14. Differenced pre-/post-earthquake DSMs undertaken after fault restoration involving a back-slip of ~4.5 m along each of the two main 2016 fault ruptures, faults 1 and 4. 'X', 'Y' and 'Z' refer to the fault blocks that were backslipped in the restoration process. Restored trench margins are shown by the black lines. Up-bulged moletracks are expressed by positive elevation changes (red colors). Location of this figure (pre-restoration) is shown by box in Figure 13E.

According to the 'deformable slat' (raft rotation) model of Little et al. (2021), the clockwise rotation of the turf rafts from a strike angle of 23° to 34° at the trench site (Figure 12b) suggests that up to 50% (~4.5 m) of the dextral-slip was accommodated by rotational deformation of the rafts in the near-surface. If so, this implies that a subequal magnitude of slip was taken up discretely by the combined strike-slip motion on faults 1 and 4.

We infer that the heave component of the coseismic fault displacement was largely accommodated by distributed deformation in the CDZ, associated with pervasive shortening and up-bulging and outward emplacement of that material (including anthropogenic backfill). At the trench site, there is no obvious fault scarp or net throw (e.g. Figure 14b), however our topographic differencing suggests that at most, 0.2 m of NW-side-up motion occurred in its vicinity. Despite this, the rupture zone accommodated ~1.3 m of fault-transverse displacement (heave). The geometry of the bulge, the oblique thrusts on its margins and its large size (e.g. Figures 8 and 9), attest to a large horizontal contraction being accommodated by deformation within (and slip along the flanks of) this bulge in the near surface. Indeed, there is more than 2 m of apparent horizontal shortening accommodated simply by reverse separation on faults A and B (Figure 8) – which is in excess of the measured heave. This conundrum of too much shortening is reinforced by our area balancing exercise, which found ~50% more deformational excess area in the bulge (Figures 10, 11) than could be explained by 2D shortening in the plane of the trench wall to absorb the known 1.3 m of heave.

This apparent excess of fault-transverse shortening can be explained simply by a rotational turf raft mechanism of distributed transcurrent deformation. As illustrated in Figure 12a, in the highly strained CDZ, the line of material points, after the earthquake, will rotate into parallelism with the logged trench wall, and must undergo 'extra' horizontal shortening – even when the overall motion across the rupture is pure strike-slip without any net heave. Where the site has experienced some heave, the rotation will impose an 'added' horizontal shortening parallel to the trench walls, leading to the perception of a greater heave than what took place. Note that this 'extra shortening' is predicted to be localised to the relatively coherent, rotated turf rafts, whereas a compensating extension is accommodated by the opening of the large open fissures between them. Our 3D topographic differencing exercise (Figure 14b) demonstrates that bulging in the rupture zone, as a whole, generated very little net deformational excess volume. It should be noted that while the base of the original trench may have acted as an artificial detachment surface (allowing the anthropogenic trench backfill to be up-bulged and deformed more easily around the trench site), the excess volume measured at the site is within error of what one would expect for the known contractional heave of 1.3 m. For a pure-strike-slip locality, one might expect nil excess volume.

Contrast in deformation style at the trench site between the last paleoearthquake (E1) and the 2016 earthquake (E0)

We hypothesised two possible explanations for the apparent contrast in ground deformation style between the 2016 earthquake and the several preceding paleoearthquakes. These paleoearthquakes (E1 – E3) involved minor extension that manifested as incremental subsidence of the central synclinal basin at the trench site during each earthquake, and slip on a central array of oblique-normal faults (Figure 4). The dip-separations on these faults were small – measured in ≤10 cm. By contrast, the 2016 earthquake created conspicuous compressional bulges within the CDZ, and inverted the former peat basin. The bulged material in places is bounded by subvertical faults (faults 1 and 4), that have dip-separations of 1–2 m, and may bifurcate upward into a ∼50 cm-wide array of splays near the surface (Figures 7 and 9). Elsewhere, along-strike, the bounding faults are convex-upward (low-angle at the surface, faults A and B in Figures 8 and 9). These structures also have large dip-separations of >1 m; slip on them (presumably dextral-reverse) carried the central plug outward across the ground surface. Interestingly, fault 4 (fault A) was not a locus of slip in the previous earthquake(s).

The simplest (and probably most important) explanation for this contrast in deformation style is that the local coseismic displacement vector at the trench site rotated clockwise in 2016 relative to that experienced during earlier earthquakes. If so, the causative reason is unknown. This rotation changed the local setting from transtensional ($\alpha < 0°$) to transpressional ($\alpha = +8°$). Analysis of the processes by which deformation was accommodated (discussed previously) and our calculated orientation of the slip vector (based on the resurveyed positions of the walls of the trench after the earthquake) indicate that transpressional kinematics in 2016 may have played a significant role in ground deformation style, as it introduced a significant contractional heave to the site. If so, the reason for this change is enigmatic.

Another possible contributing explanation for this contrast – not mutually exclusive to the first – is that there was a change in mechanical soil properties between the previous earthquake and 2016. Such a change could conceivably have been triggered by the introduction of exotic grasses at the time of European arrival, leading to a stiffer, more tightly bound and less granular soil, and/or to a more cohesive or clay-rich layer of sediments in the near-surface. If so, this change might have promoted the formation of coherent turf rafts, followed by their clockwise rotation, shortening and consequent up-bulging to form mole-tracks in 2016. Ongoing paleoenvironmental and palynological work (L. Petherick, pers. comm., 2020; and manuscript in preparation) is focused on samples of the several peaty layers of the central depression, as these represent the respective topsoils during the last three paleoearthquakes (units *lp*, *mp* and *up*), and the 2016 earthquake (unit *ts*) at this site. Preliminary results (pers. comm., L. Petherick, 2020) show that the relative abundances of pollen species assemblages have not changed much over the last 1000 years. This suggests that the mechanical properties of the near surface sediment and soil have likely remained relatively stable since the late Holocene. Additional information on grainsize distributions and moisture content of these peats may clarify whether or not the strength and cohesion of the soil have changed significantly since the last paleoearthquake.

Expression of large magnitude strike-slip rupture in a fault perpendicular plane of view

Ancient strike-slip earthquakes on this section of the Kekerengu Fault consistently accommodated fault-orthogonal extension (i.e. transtension), manifested in T1 as dm-scale normal dip-separations of the stratigraphic units that infilled the incrementally subsiding axial depression (basin) across the fault trace. By contrast, the post-2016 T1 logs showed a large fault-perpendicular shortening in the trenches, a deformation that was in part expressed by dip-separations of up to ∼2 m on the main faults rupturing the ground in 2016 (Figures 7 and 9). Despite this, dip separations on the reactivated, dominantly strike-slip faults in the displaced trench walls were mostly small – only a few cm – despite the out-of-plane displacements being up to several metres (in Figure 7: units *uc* and *lp* on fault 1; in Figure 9, unit *psp* on fault 4).

This demonstrates that large strike-slip displacements are commonly expressed as only cm-dm scale dip separations in a fault-perpendicular plane of view (Sieh 1984 Fumal et al. 1993;) especially where material are flat-lying and laterally continuous along the strike of the fault (and so its infill is relatively homogenous or unchanging in that direction). Small dip separations are particularly to be expected, moreover, where the overall slip was transtensional, because the typical lack of folding associated with such motion will not introduce (or amplify) any out-of-plane changes in stratal dip that can be converted by strike-slip into large dip-separations on trench walls. This suggests that the several previous earthquakes on the Kekerengu Fault may well have accommodated similarly large strike-slip magnitudes as in 2016, but that they were only expressed as dm-scale vertical offsets. Where the fault motion has been pure-strike-slip or transpressional, more bulging and folding will deform the near surface materials – especially if they are coherent and form 'rafts.' Depending on the 3D geometry and continuity of the surface units, and the orientation of the trench, such motions may lead to larger dip separations expressed on trench walls. Without pre-knowledge of the actual 2016 displacement vector at the trench site, one might have misinterpreted the large fault-orthogonal contraction (>2 m, e.g. Figure 10) and bulging as evidence for an earthquake that accommodated a large component of reverse slip and also throw. In reality, the heave was ∼1.3 m and the net throw across the fault <20 cm.

Finally, the post-earthquake trench logs also illustrate that fault-perpendicular cross-cutting relationships can be the result of a progression of structures developing (possibly over just seconds) during a single earthquake, rather than evidence for multiple earthquakes. This is exemplified in Figure 9, where fault 1 is inferred to have initially ruptured in 2016 as an open fault fissure on the ground surface (probably a Riedel fault), which then infilled with surface topsoil (unit *bp* yielding a modern ^{14}C age). Subsequently, the raft of material bounded by this structure probably rotated coseismically about a vertical axis, during which the rafts were forced to shorten (Figure 12a), activating oblique thrust faults (faults 1A and 1B). These thrusts overrode and sealed the previously formed fissure, and displaced older stratigraphic units overtop it (units *ml*, *o* and *ts*). The several fault strands involved are locally cross-cutting, yet they probably moved at intervals only seconds apart.

Conclusions

During the 2016 Mw 7.8 Kaikōura earthquake, a pre-existing paleoseismic trench was dextrally displaced by ∼9 m and experienced contractional heave of 1.3 ± 0.4 m – the largest globally recorded displacement of a paleoseismic trench. The 2016 coseismic slip was transpressional, with the slip vector trend of +8° clockwise to the local fault strike, whereas the several most recent paleoearthquakes were uniformly transtensional (negative angle), suggesting a change in the local fault kinematics. Our data sets reveal a <3.5 m wide central deformation zone at the site that was up-bulged, broken into elongate rafts by Riedel faults (now clockwise-rotated), internally strongly sheared and deformed, and bound by two steeply dipping surface rupturing faults.

While we cannot measure the exact partitioning 'budget' of strike-slip between (1) distributed rigid-body rotation and shortening of turf rafts plus distributed shearing in the CDZ; versus, (2) discrete slip accrued along the two marginal faults, our analysis suggests these deformation mechanisms accomplished a subequal magnitude of dextral-slip within the top 2 m of surficial sediment and soil, with mechanism (1) probably preceding (2) during the earthquake. The marginal faults formed through reactivation of pre-existing, upward terminating faults, and probably dominated the slip budget once they reached the surface. At least one of these marginal faults (fault 4) was not the locus of slip in the previous earthquake(s), suggesting that faults should be defined as zones large enough to accommodate such unpredictability.

Near the ground surface, the contractional heave component of motion was absorbed by up-bulging of the CDZ, together with thrust-like outward emplacement of that central bulge. The amount of horizontal shortening (perpendicular to the fault, parallel to the trench walls) accommodated was approximately double the magnitude of heave. This discrepancy is explained by the rotational motion of the turf rafts, requiring them to shorten as they approach perpendicularity with the fault. This out-of-plane motion generates additional shortening and deformational area in a given plane to that imposed by the heave.

The expression of large magnitude strike-slip earthquakes in cross-section can vary significantly between earthquakes. Transtensional ruptures, even where the strike-slip component of slip is many metres, may yield discrete dip-separations of stratigraphic units on trench walls that are only a few centimetres, whereas, strike-slip or transpression may yield a several meter-wide zone of distributed deformation (including bulging) near the centre of the rupture zone, generating much larger, albeit variable (and in some cases still small) stratigraphic offsets in the process.

Cross-cutting fault strands in a trench may form at different instants during a single earthquake, with the potential for this happening increasing, we suspect, as displacement increases.

Acknowledgements

Thanks are extended to the reviewers of this paper – John Begg, and an anonymous second reviewer, as well as Rob Langridge and Carolyn Boulton for their comments on an earlier version of the manuscript. We also thank Andy Nicol, the editor of this journal. Thanks is also extended to the EQC (grant 18-758) for funding this research project. We also thank Jessie Vermeer, Emma Watson and Lynda Petherick for their help in the trenching expedition of February 2018.

Disclosure statement

No potential conflict of interest was reported by the author(s).

Funding

This work was supported by Earthquake Commission [grant number 18/758].

Data availability

The supplemental files cited in this paper along with any other data that support the findings of this study are openly available in figshare at https://doi.org/10.6084/m9.figshare.14888892.v1.

ORCID

Philippa Morris http://orcid.org/0000-0001-7720-2012
Matthew Hill http://orcid.org/0000-0002-1818-1458
Kevin Norton http://orcid.org/0000-0002-7995-6464

References

Fumal TE, Schwartz DP, Pezzopane SK, Weldon RJ. 1993. A 100-year average recurrence interval for the San Andreas Fault at Wrightwood, California. Science. 259(5092):199–203.

Haller KM, Crone AJ, Wood SH.. 2004. Twenty years after the Borah Peak earthquake: Field guide to surface-faulting earthquakes along the Lost River fault, Idaho. In: Haller KM, Wood SH, editors. Geological Field Trips in Southern Idaho, Eastern Oregon, and Northern Nevada, U.S. Geol. Surv. Open-File Rept. 2004–1222; p. 116–133.

Hill M, Ashraf S. 2017. Digital surface models from Clarence to Kekerengu using semi-global matching and structure from motion photogrammetry and their use in geomorphic interpretation, GNS Science Report; 2017/17, GNS Science, Lower Hutt, New Zealand.

Kearse J, Little TA, Van Dissen RJ, Barnes PM, Langridge R, Mountjoy J, Hemphill-Haley M. 2018. Onshore to offshore ground-surface and seabed rupture of the Jordan–Kekerengu–Needles fault network during the 2016 M w 7.8 Kaikōura earthquake, New Zealand. Bulletin of the Seismological Society of America. 108 (3B):1573–1595.

Litchfield NJ, Villamor P, Dissen RJV, Nicol A, Barnes PM, Barrell DJA, Zinke R. 2018. Surface rupture of multiple crustal faults in the 2016 M w 7.8 Kaikōura, New Zealand, Earthquake. Bulletin of the Seismological Society of America. 108(3B):1496–1520.

Little TA, Morris P, Hill MP, Kearse J, Van Dissen RJ, Manousakis J, … Howell A. 2021. Coseismic deformation of the ground during large-slip strike-slip ruptures: Finite evolution of "mole tracks". Geosphere.

Little TA, Van Dissen R, Kearse J, Norton K, Benson A, Wang N. 2018. Kekerengu fault, New Zealand: timing and size of late Holocene surface ruptures. Bulletin of the Seismological Society of America. 108(3B):1556–1572.

Morris P. 2020. Accommodating~ 9 m of dextral slip on the Kekerengu Fault through ground deformation during the Mw 7.8 Kaikōura Earthquake, November 2016.

Shirahama Y, Yoshimi M, Awata Y, Maruyama T, Azuma T, Miyashita Y, Miyakawa A. 2016. Characteristics of the surface ruptures associated with the 2016 Kumamoto earthquake sequence, central Kyushu, Japan. Earth, Planets and Space. 68(1):1–12.

Sieh KE. 1984. Lateral offsets and revised dates of large prehistoric earthquakes at Pallett Creek, southern California. Journal of Geophysical Research: Solid Earth. 89 (B9):7641–7670.

Stirling MW, Litchfield NJ, Villamor P, Van Dissen RJ, Nicol A, Pettinga J, Zinke R. 2017. The Mw7. 8 2016 Kaikōura earthquake. Bulletin of the New Zealand Society for Earthquake Engineering. 50(2):73–84.

Zekkos D, Manousakis J, Athanasopoulos-Zekkos A, Clark M, Knoper L, Massey C, Archibald G, Greenwood W, Hemphill-Haley M, Rathje E, et al. 2018. Structure-from-motion based 3D mapping of landslides & fault rupture sites during 2016 Kaikoura earthquake reconnaissance. In Eleventh U.S. National Conference on Earthquake Engineering – Integrating Science, Engineering & Policy, June 25–29. Los Angeles, CA.